Journal of
Composites Science

MDPI

Article

Controllable Synthesis of Graphene-Encapsulated NiFe Nanofiber for Oxygen Evolution Reaction Application

Mengyang Li [1,†], Jiayi Rong [1,†], Ning Guo [1], Susu Chen [1], Meiqi Gao [1], Feng Cao [1,*] and Guoqing Li [2,*]

[1] Key Lab for Anisotropy and Texture of Materials (MoE), School of Materials Science and Engineering, Northeastern University, Shenyang 110819, China; 2100534@stu.neu.edu.cn (M.L.); 20182924@stu.neu.edu.cn (J.R.); guoning_0226@163.com (N.G.); 17854173815@163.com (S.C.); gaomq@smm.neu.edu.cn (M.G.)
[2] Department of Materials Science and Engineering, North Carolina State University, Raleigh, NC 27695, USA
* Correspondence: caof@atm.neu.edu.cn (F.C.); gli4@ncsu.edu (G.L.)
† These authors contributed equally to this work.

Abstract: Carbon-Encapsulated NiFe Nanofiber Ni_xFe_y@C-CNFs have been demonstrated to be promising candidates to replace conventional nobel metals-based catalysts for oxygen evolution reaction. Here, we developed a facile method of electrospinning and high temperature carbonization to synthesize Ni_xFe_y@C-CNFs catalysts. It is proved that Ni_3Fe_7@C-CNFs exhibited low overpotential (245 mV) and excellent stability in alkaline electrolyte for OER. This work provides a good platform for the synthesis and design of graphene-encapsulated alloy catalysts.

Keywords: graphene-encapsulated; electrospinning; OER; nanoparticles

Citation: Li, M.; Rong, J.; Guo, N.; Chen, S.; Gao, M.; Cao, F.; Li, G. Controllable Synthesis of Graphene-Encapsulated NiFe Nanofiber for Oxygen Evolution Reaction Application. *J. Compos. Sci.* **2021**, *5*, 314. https://doi.org/10.3390/jcs5120314

Academic Editor: Francesco Tornabene

Received: 30 October 2021
Accepted: 26 November 2021
Published: 29 November 2021

1. Introduction

Oxygen evolution reaction (OER) is one of the most basic and important electrochemical reactions for the production of renewable energy, which can be used in many green energy systems such as water splitting, fuel cells and metal-air batteries [1,2]. The multi-electron transfer reaction mechanism makes it challenging to develop such highly efficient catalysts [3,4]. Noble metals oxides (RuO_2/IrO_2) have been used as OER catalysts in practical applications [5,6]. However, poor stability, low selectivity and high cost hinder their large-scale development [7]. Therefore, there is an urgent need to develop efficient OER non-noble metal electrocatalysts. Researchers demonstrated that transition metal (TM) with empty d-electron orbital participates in the reaction as catalyst [8,9]. In particular, Ni-based transition metals are highly efficient OER catalysts [10,11]. The researchers improved the electrocatalytic properties of Ni by alloying with other metals, hydroxylation, and forming compounds with nonmetal based on non-nobel metals [12,13]. In addition, graphene layers encapsulated metal or metal alloy nanoparticles is an effective method to improve the activity and stability of OER catalyst [14–17]. Thereby, it is a promising strategy to encapsulate Ni-based transition metals alloys in a graphite layer [18,19]. By doing so, not only the synergistic effects between the graphite shell and the NiFe nanoparticles core enhance the OER activity, but also the graphene shell can protect the alloy from the corrosion of alkaline electrolyte [15,17,20].

Although graphene layers encapsulated metal materials have been widely studied, there is still a lack of an effective method to synthesize them. First of all, the composition and proportion of the core metal is difficult to accurately control [21,22]. Secondly, the size of graphene layers encapsulated metal nanoparticles and the thickness of carbon layer are difficult to meet the expected requirements [23]. Finally, the activity and stability of the catalysts cannot be guaranteed [24]. Therefore, it will be of great interest to develop a more facile method to synthesize graphene layers encapsulated metal materials.

Herein, we report a simple method to synthesize graphene layers encapsulating Ni_3Fe_7 alloy materials supported by carbon nanofibers (Ni_3Fe_7@C-CNFs) by electrospinning and subsequent high temperature carbonization. In this way, we can precisely control the proportion of the core metal. The nanoparticles were about 12 nm in size and distributed uniformly along the carbon nanofibers. In the alkaline OER reaction, Ni_3Fe_7@C-CNFs shows excellent catalytic activity, the overpotential is only 245 mV to reach the current density of 10 $mA \cdot cm^{-2}$, even better than that of the commercial catalyst RuO_2. Moreover, the Tafel slope of Ni_3Fe_7@C-CNFs is only 67 $mV \cdot dec^{-1}$ and it has a relatively fast chemical kinetics. In addition, the catalyst has long-term stability. This work provides a possible way for the design and synthesis of OER catalysts.

2. Materials and Methods

2.1. Materials

Nickel nitrate hexahydrate (Ni $(NO_3)_2 \cdot 6H_2O$), ferric nitrate nonahydrate ($Fe(NO_3)_3 \cdot 9H_2O$), N,N-dimethylformamide (DMF) and polyvinylpyrrolidone (K30) were purchased from Sinopharm Chemical Reagent Co., Ltd., Shanghai, China. Anhydrous ethanol and potassium hydroxide were purchased from Yongda Chemical Reagent Co., Ltd., Tianjin, China. The Nafion solution was purchased from Minnesota Minerals and Manufacturing Company. All chemical reagents are of analytical grade and no further purification is required.

2.2. Preparation of Ni_xFe_y@C-CNFs

The brown precursor solution with a certain viscosity was obtained by adding 2 mmol of nitrate and 5.6 g PVP to 10 mL DMF and stirring at a constant speed for 12 h. The prepared precursor solution was slowly inhaled into a 20 mL Syringe. Then switch on the injection pump at the rate of 0.5 mL/h. When the temperature reaches 30 °C, turn on the high voltage power supply, adjusting the voltage to 17 kV, and observe that there were fine fibers sprayed on the aluminum foil paper. After 12 h of spinning, the nanofiber precursor was obtained. The precursor was pre-oxidized in muffle furnace. It was heated to 250 °C at the rate of 1 °C/min in the air, and then furnace cooled to room temperature. The pre-oxidized nanofiber precursor was carbonized at high temperature in a tube furnace with a heating rate of 5 °C/min to 800 °C for 2 h. After grinding and sieving, it was installed in the sample tube and sealed for spare.

2.3. Preparation of Ni_xFe_y@C-CNFs Electrode

During the electrochemical performance test, the catalyst samples need to be uniformly loaded on the carbon paper electrode. Cut the carbon paper into a small rectangle of $1 \times 1.5\ cm^2$, bond the wires and the carbon paper together with conductive silver glue, letting it dry completely in the air for an hour. Take the same amount of A and B glue and mix them evenly. Cover the conductive silver glue on both the front and back and apply it around to form a groove. Weigh 5 mg of the catalyst to be tested, add 600 μL of ultrapure water, 200 μL of absolute ethanol and 10 μL of Nafion solution, sonicating for 30 min to make the sample uniformly dispersed. Finally, use a pipette to suck 30 μL of the catalyst solution into the groove part of the carbon paper, when it is completely dried out, repeatting the dripping five times. And then perform the electrochemical performance test after it is completely dried.

2.4. Material Characterization

X-ray diffraction (XRD) is an effective means to determine the crystal structure of materials. The phase constitutions of the alloys were examined by Smartlab X-ray diffraction from Japanese company Rigaku. The test working current is 200 mA and the working voltage is 40 kV, with Cu Kα Ray (λ = 1.54 Å) as the incident source, filtered by graphite monochromator, using θ/2θ, the linkage mode is used for continuous scanning in the range of 10–90°, and the scanning speed is 5°/min.

Scanning electron microscopy (SEM) can interact with materials through incident electrons, and then obtain the morphology information of materials. The field emission scanning electron microscope JSM-7001F produced by Japan Electronics Corporation (JEOL) was used in this experiment to obtain surface morphology.

Transmission electron microscopy (TEM) is a method to observe more detailed crystal structure and phase composition. In this experiment, JEM-2100F transmission electron microscope produced by Japan Electronics Corporation (JEOL) was used to obtain the information of material morphology and crystal structure.

2.5. Electrochemical Measurements

The electrochemical measurements using IM6e electrochemical workstation produced by Zahner company of Germany were carried out by a standard three-electrode cell in 1 M KOH solution (without oxygen). Among them, the glassy carbon electrode is the working electrode, the mercury oxide (Hg/HgO) electrode is the reference electrode, and the carbon rod is the counter electrode.

During the Linear voltammetric scanning (LSV) test, the scanning rate is 5 mV/s, the voltage range of the oxygen evolution reaction (OER) is 0.1–1.1 V. Tafel slope is calculated from LSV polarization curve according to the equation as follow:

$$\eta = a + b \log j \quad (1)$$

where j was the current density, b was the Tafel slope, η was the overpotential.

Electrochemical surface areas (ECSA) is proportional to the electric double layer capacitance (Cdl) of the electrode. Cdl is measured by cyclic voltammetry curve, and the appropriate potential range is selected in the non-Faraday zone, with 10, 20, 30, 40, 50 $mV \cdot s^{-1}$ speed, scan 20 circles, read the current density difference at a specific potential, plot with the scan speed, and the slope of the curve obtained by fitting is the electric double layer capacitance.

Electrochemical impedance spectroscopy (EIS) can be used to measure the impedance of the catalyst under applied voltage, which can reflect the speed of electron transfer. The disturbance potential is set at 5 mV, and the frequency range is set from 100 MHz to 100 kHz.

Electrochemical stability test: In this experiment, the electrochemical stability test is to maintain the sample at Constant potential for 12 h in the i-t working mode of the electrochemical workstation, and observe the current density change of the sample.

The electrochemical experiments were all conducted at room temperature.

The reference electrode was calibrated to reversible hydrogen potential (RHE)using platinum electrode for both working and counter electrodes and converted into RHE according Nernst equation RHE = 0.0591 pH + 0.197.

3. Result and Discussion

3.1. Characterizations of Samples

Ni_xFe_y@C-CNFs is synthesized by a simple and versatile method using electrospinning and subsequent heat treatment, as shown in Figure 1. Firstly, the metal salt was dissolved in DMF, and then PVP was added to form the spinning solution. The precursor was electrospun from the prepared spinning solution mixture. Then Ni_xFe_y@C-CNFs was obtained by pre-oxidation and high temperature carbonization of the precursor.

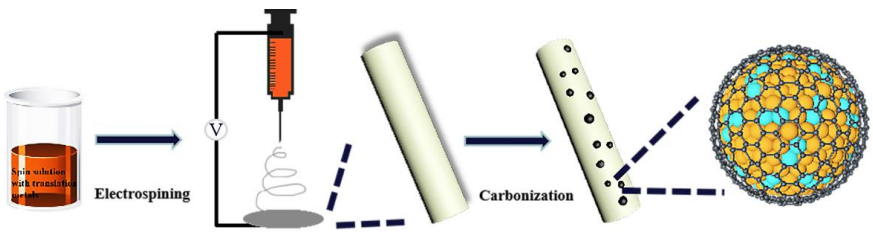

Figure 1. Schematic illustration of the synthesis process of the Ni_xFe_y@C-CNFs.

The controllable synthesis and compositions are confirmed by XRD measurements as Figure 2. Compared with the diffraction peaks of Ni and Fe, the diffraction peaks of NiFe alloy shift to some extent, which proves the formation of the alloy structure. The Ni_3Fe_7@C-CNFs samples showed characteristic peaks at 43.7°, 51.0°, and 74.8°, corresponding to the (111), (200) and (220) faces of the NiFe alloy, respectively. Except for the characteristic diffraction peaks corresponding to face centered cubic phase alloy, there are no other diffraction peaks, which proves that there are only single-phase alloys. The magnified portion of XRD pattern in the 2 θ range of 42–48° is provided on the right. The strongest diffraction peak shifts slightly at a small angle in a regular trend with the change of alloy composition, which proves that the lattice constant changes due to the formation of ideal alloy structure. All the composites show a major peak at 2 θ = 26°, corresponding to the typical (002) plane of graphitic carbon.

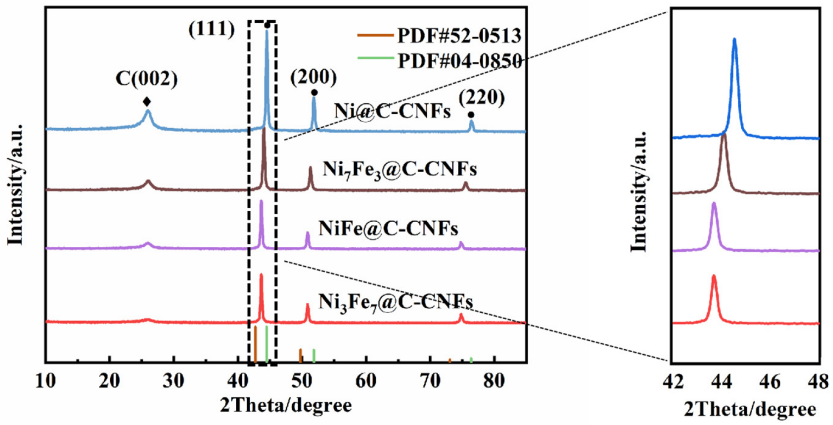

Figure 2. XRD patterns of Ni_xFe_y@C-CNFs and magnified portion in the 2 θ range of 42°–48°.

After mixing the nitrate solution and the PVP uniformly, the precursor of NixFey@C-CNFs can be formed after electrospinning for 12 h. As shown in Figure 3a, the SEM morphology of the prepared precursor was characterized, from which the produced nanofibers have a diameter of about 100 nm. The surface of carbon nanofibers is smooth and its morphology is uniform. Figure 3b shows that the precursor remains fibrous after high temperature carbonization, at which point the fiber becomes a highly conductive carbon material. Carbon nanofibers have the advantages of small size, large specific surface area and large aspect ratio. Therefore, electrons and protons can transfer in a controlled direction. However, compared with the precursors before high temperature treatment, the surface of the nanofibers is no longer smooth. It can be clearly observed that both the inner and surface of the carbon nanofibers are formed into round alloy particles. The nano-alloy particles adhere uniformly, and there is no obvious agglomeration of the alloy particles. At the same time, to determine the distribution of each element in the prepared sample, part of the region was selected for mapping detection in the experiment. The Ni and Fe elements in the sample are evenly distributed, and there is no obvious element agglomeration, indicating that the formation of single-phase alloys as shown in the illustration.

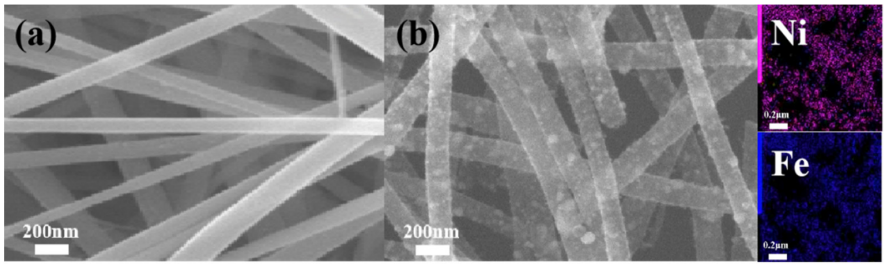

Figure 3. (**a**) SEM images of Precursor; (**b**) SEM images of Ni_3Fe_7@C-CNFs and the corresponding elemental mapping of Ni_3Fe_7@C-CNFs.

To clarify the Ni_xFe_y@C-CNFs crystal structure and the nano particle size distribution, TEM images were analyzed further. Computer software Nano Measurer was used to count and calculate the nano particle size distribution. First, the scale is specified by selecting the length in the imported figure and setting the actual length and unit (Figure 4a). Next, select the particles in the figure one by one and their lengths will be automatically recorded and stored. Finally, the statistical table of nano particle sizes and the distribution figure are exhibited. The results show that metal alloy particles with a size of about 12 nm are distributed along the inside and outside of the carbon nanofibers uniformly (inset in Figure 4a). The size of alloy particles is small and the specific surface area is large, which provides rich active sites for catalytic reaction. A nano particle growing on carbon nanotubes was selected for observation, and the core-shell structure could be clearly observed again. High-resolution transmission electron microscopy (HRTEM) characterization of the Ni_3Fe_7@C-CNFs indicates that the alloy particles are completely encapsulated by the graphene layer (the red curve area) with a thickness of 3.2 nm (Figure 4b). Not only can the core—shell structure separate the alloy from the external electrolyte to avoid the corrosion of the alloy in a strong alkaline environment, but also it will prevent the agglomeration of alloy particles in the reaction process to improve the stability of the catalyst.

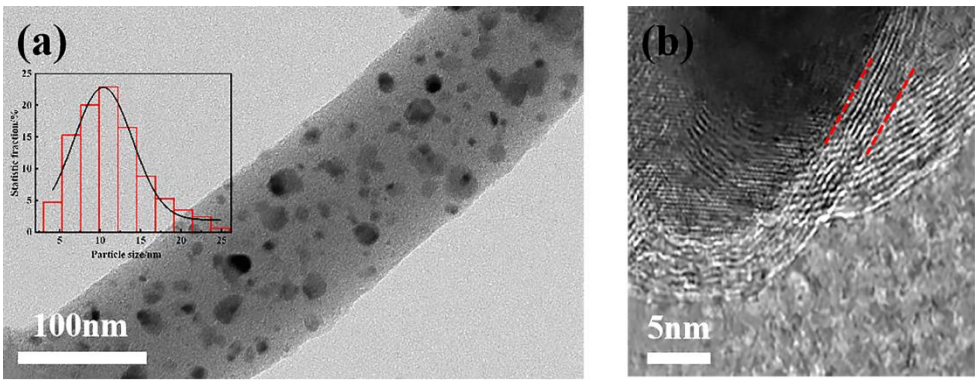

Figure 4. (**a**) TEM image (the inset shows Particle size distribution); (**b**) HRTEM image of Ni_3Fe_7@C-CNFs.

3.2. Electrochemical Analysis

The electrocatalytic OER activity of the catalysts is investigated in Nitrogen saturated alkaline solution (1 M KOH) in a standard three-electrode system. The polarization curves of LSV are shown in Figure 5a. At a current density of 10 mA cm^{-2}, the overpotential of Ni@C-CNFs is the highest 348 mV. Then the metal element Fe is introduced to form Ni-Fe alloy. Compared with pure nickel, the over-potential of bimetallic alloys has a decreasing tendency, which indicates introducing Fe into Ni can improve the OER catalytic performance. In addition to the necessity of qualitative analysis of the existence of Fe, we also designed experiments to quantitatively analyze the influence of Fe on the catalytic activity. We designed NiFe alloys with different proportions of Ni_7Fe_3@C-CNFs, NiFe@C-CNFs and Ni_3Fe_7@C-CNFs. As shown in Figure 5b, it can be observed visually the overpotential of Ni_3Fe_7@C-CNFs (245 mV), is better than NiFe@C-CNFs (308 mV) and Ni_7Fe_3@C-CNFs (300 mV). In addition, we also tested commercial catalyst RuO_2, the results show that the catalytic activity of Ni_3Fe_7@C-CNFs is even better than RuO_2 (290 mV). Previous studies and relevant calculations show that adjusting the proportion of the core metals is an effective means to adjust the catalytic performance [25–29]. The main effect is that the difference of Ni/Fe ratio leads to the transfer of electrons to the active sites on the catalyst surface, which increases the free energy of O *, making it easier to be adsorbed and desorbed, which reduce the over-potential of OER reaction. This is consistent with the results of our OER electrochemical measurements. When the ratio is 3/7, the catalyst has the lowest Tafel slope (67.0 mV dec^{-1}) and the charge-transfer resistance (Figure 5c), suggesting that introduction of different ratio of NiFe affects the kinetics of the electrode

reactions. The catalyst of Ni_3Fe_7@C-CNFs has the largest electrochemical double-layer capacitance (73.02 mF cm^{-2}) indicating that the maximum number of active sites are on its surface among the five catalysts. To verify the synergistic effect of graphene and metal core can significantly affect the catalytic performance, Ni_3Fe_7 alloy without graphene and the carbon fiber, which did not support any metals or alloys were prepared respectively for comparison. The electrochemical test results indicated the bare carbon fiber sample did not show any catalytic activity. Thus, the positive effect of carbon fiber on performance can be excluded. The OER activity of the prepared samples with graphene layer removed decreases greatly, which indicates that the synergistic effect of graphene and metal core is the main reason for the improvement of its activity. According to previous relevant studies, the transfer of electrons from the core metal to graphene and the increase of the electron density of states near the Fermi level is one of the main reasons for the materials [30]. Graphene encapsulated transition non noble metal catalyst can effectively reduce the reaction energy barrier of each unit of OER reaction by adjusting the electronic structure of outer graphene through the inner metal to reduce OER overpotential and enhance the activity of the catalyst [19]. Thus, it can be concluded that the excellent catalytic performance results from the transfer of electrons from the internal metal to graphene shell. The study has proved that changing the relative proportion of metals in the alloy is a common method, which can provide a greater opportunity to change the catalytic activity. The electronic structure of the carbon shell can be adjusted by changing the proportion of the core metal, so as to optimize the catalytic activity [26]. In order to have a more comprehensive understanding of the electrocatalytic properties of the catalysts, we fit the Tafel slope from the LSV curve (Figure 5c). This value can be used to reflect the reaction kinetics of materials in catalytic reaction. The Tafel slope of Ni_3Fe_7@C-CNFs is 67.0 mV dec^{-1}, which is smaller than that of Ni@C-CNFs (82.9 mV dec^{-1}), NiFe@C-CNFs (79.1 mV dec^{-1}), and Ni_7Fe_3@C-CNFs (73.8 mV dec^{-1}). Thus, the catalyst Ni_3Fe_7@C-CNFs has the fastest reaction kinetics of our ferronickel alloy catalysts for the OER application. In order to further determine how graphene can enhance their performance on its OER activity, the electrochemical reaction kinetics of the sample was analyzed by Tafel slope. Figure 5c shows the Tafel curve. It can be seen that removing the graphene can increase its Tafel slope and bring a negative effect. It is inferred that after the graphene capsulated alloy structure is formed, the electronic structure is optimized due to the transfer of electrons from the internal metal to graphene, to accelerate the OER kinetic rate. It is inferred that after the graphene encapsulated alloy structure is formed, the electronic structure is optimized due to the transfer of electrons from the internal metal to graphene, so as to accelerate OER kinetic rate. Optimizing the Ni/Fe ratio can further reduce the Tafel slope, which shows that the ability of electron transfer to graphene can be adjusted by changing the internal alloy composition [14]. The electronic coupling between the internal alloy and graphene accelerates its kinetic rate, which is also one of the main reasons for the improvement of its OER activity. In addition, when compared with the recently reported OER electrocatalysts (Figure 5d), the Ni_3Fe_7@C-CNFs exhibit the remarkable activity with low overpotential at 10 mA cm^{-2} of 245 mV. All the compared electrocatalysts were summarized in Table S1.

The source of the differences between NiFe alloy catalysts with different Ni/Fe ratios in OER activity can be further explored through the change of electrochemical active area. Since the electrochemical surface areas (ECSA) are proportional to the electric double layer capacitance (C_{dl}) of the electrode, the ECSA can be expressed by C_{dl}. The CV curves of Ni_3Fe_7@C-CNFs at different scanning rates are shown in Figure 6a. The others are shown in Figure S1. All samples were subjected to CV cycle under the same conditions, and the electrochemical active area could be obtained by data processing and fitting (Figure 6b). Compared with the others catalysts, the electric double layer capacitance of Ni_3Fe_7@C-CNFs is the largest, which is 73.02 mF cm^{-2}. Large electrochemical active area can provide abundant active sites for catalytic reaction. How graphene can enhance their performance can be further explored through the change of electrochemical active area. Ni_3Fe_7@C has the larger electrochemical active area than Ni_3Fe_7 alloy, indicating that electrons transferred

from the internal metal to the outer layer graphene, activating more active sites, to improve its OER activity. Subsequently, the electrochemical impedance spectroscopy (EIS) of the samples was measured to further explain the difference of charge transfer ability between different catalysts. The surface kinetics and conductivity of the catalyst can be analyzed by impedance spectroscopy. All samples show a small charge transfer resistance Rct, and its change trend is consistent with the polarization curves of LSV, Tafel slope and the electrochemical surface areas of the corresponding electrode. Ni_3Fe_7@C-CNFs has the smallest charge transfer resistance in comparison with others, which means that it has faster interfacial charge transfer efficiency and reaction kinetic rate. From the Figure 6c, Ni_3Fe_7 alloy without graphene sample exhibited a larger charge transfer resistance, which means it has lower interfacial charge transfer efficiency and reaction kinetic rate and has a negative effect on OER catalytic activity. The above comparison results between Ni_3Fe_7 alloy and Ni_3Fe_7@C-CNFs show that the electronic coupling between the internal alloy and graphene accelerates its kinetic rate, which is also one of the main reasons for the improvement of its OER activity.

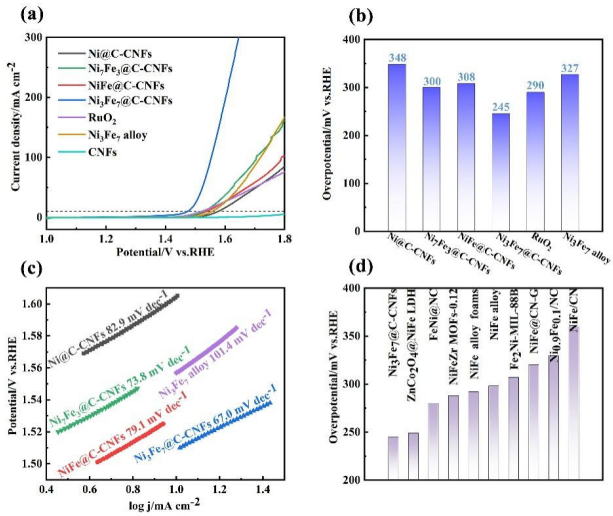

Figure 5. (**a**) LSV polarization curves after iR correction; (**b**) The overpotentials obtained from polarization curves at the current density 10 mA cm^{-2}; (**c**) The corresponding Tafel plots; (**d**) Comparison of overpotentials at 10 mA cm^{-2} of Ni_3Fe_7@C-CNFs with reported literatures.

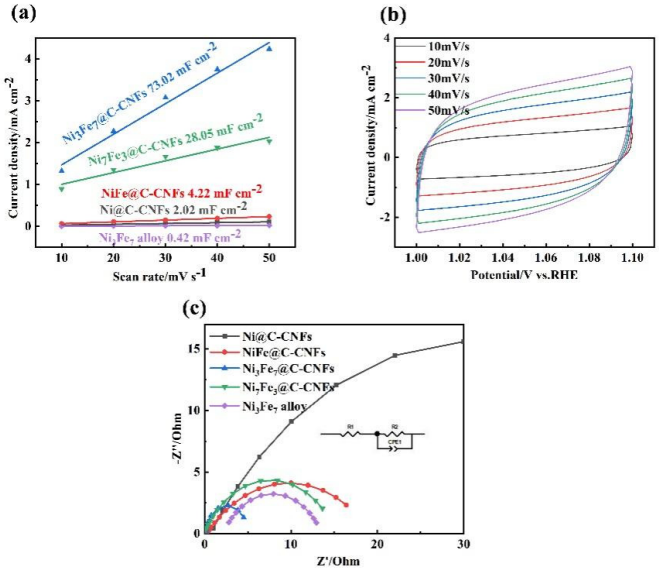

Figure 6. (**a**) Cyclic voltammetry curves of samples; (**b**) ECSA measurements under different treatment conditions; (**c**) Nyquist plots.

Researchers have tended to focus on decreasing the overpotential when designing catalysts, while focusing less on the stability. In addition to the catalytic activity, the stability is also a necessary condition to judge the performance of the catalyst. We tested the i-t curve of the sample Ni_3Fe_7@C-CNFs by potentiostatic method, as shown in Figure 7a. It can be seen from the figure that the current density of the sample hardly decreased after 12 h test at high current density of 100 mA cm^{-2}. The LSV curve before and after stability is almost consistent, which indicates that Ni_3Fe_7@C-CNFs has excellent stability (Figure 7b). The stability of the sample after scanning electron microscope characterization, as shown in Figure 7c. The morphology of the carbon fiber-loaded alloy was not destroyed after the stability test, which showed that Ni_3Fe_7@C-CNFs had excellent properties and morphological stability. The good stability results from the core-shell structure. The carbon shell can not only prevent the agglomeration of the nanoparticles, but also separate the inner alloy from the strong alkaline environment of the electrolyte. Therefore, its excellent activity and good stability make it possible to replace the practical application of noble metal based electrocatalysts in OER.

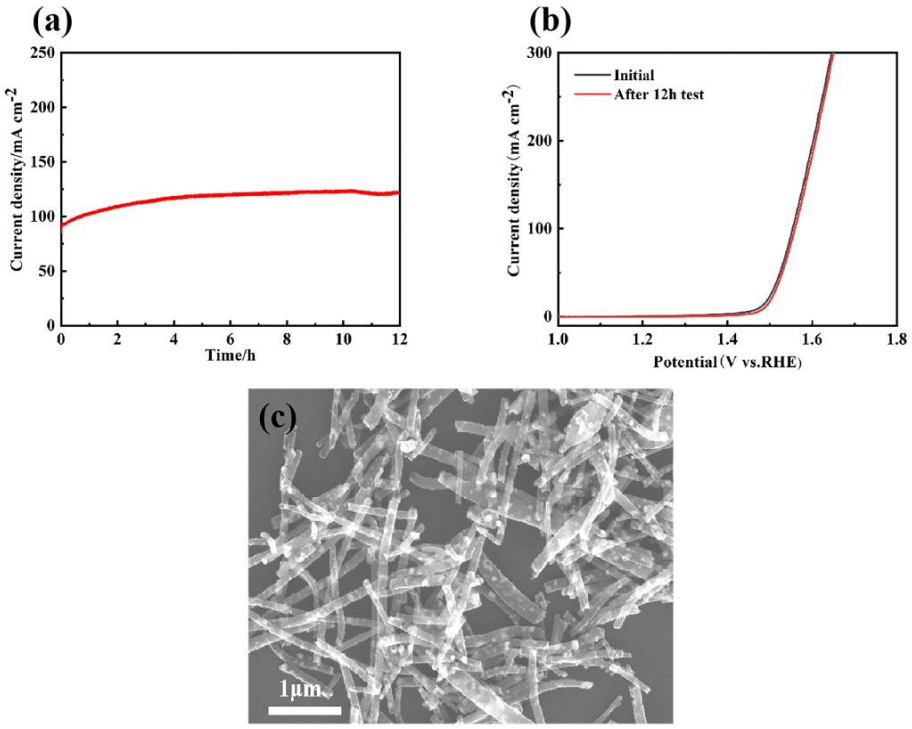

Figure 7. (**a**) LSV image after stability test; (**b**) i-t image; (**c**) SEM image after stability test.

4. Conclusions

In this paper, Ni_xFe_y@C-CNFs catalysts for OER were prepared by a facile method of electrospinning combined with pre-oxidation and high temperature carbonization. This method can precisely regulate the compositions of different samples. Due to the synergistic effects of NiFe nanoparticles metal core and the graphene layer, superior OER activity was achieved successfully. By adjusting the proportion of Ni and Fe, it is proved that Ni_3Fe_7@C-CNFs exhibited excellent catalytic performance for OER in 1.0 M KOH with an overpotential of 245 mV to reach a current density of 10 mA cm^{-2}. After 12 h reaction, the LSV curve can still coincide with the one before reaction, and there is no obvious decline, which proves that it shows remarkable stability. This work provides a new idea for OER application of nano particles prepared by electrospinning combined with pre-oxidation and high temperature carbonization and broadens the horizon of design graphene-encapsulated alloy catalysts.

Supplementary Materials: The following are available online at https://www.mdpi.com/article/10.3390/jcs5120314/s1, Figure S1: Cyclic voltammetry curves of other Ni_xFe_y@C-CNFs. (a) Ni@C-CNFs. (b) NiFe@C-CNFs. (c) Ni_7Fe_3@C-CNFs; Table S1: Electrocatalytic performance comparison of reported electrocatalysts.

Author Contributions: Methodology, experiment, validation, writing—original draft preparation, writing—review and editing, M.L. and J.R.; investigation, resources, and data curation, N.G., S.C. and M.G.; conceptualization, visualization, supervision, project administration, and funding acquisition, F.C. and G.L. All authors have read and agreed to the published version of the manuscript.

Funding: This research was funded by National Training Program of Innovation and Entrepreneurship for Undergraduates, grant 201910145104, and "the Fundamental Research Funds for the Central Universities", grant N182410001.

Acknowledgments: (1) Project 201910145104 supported by National Training Program of Innovation and Entrepreneurship for Undergraduates. (2) Supported by "the Fundamental Research Funds for the Central Universities" (N182410001).

Conflicts of Interest: The authors declare no conflict of interest.

References

1. Song, J.J.; Wei, C.; Huang, Z.F.; Liu, C.; Zeng, L.; Wang, X.; Xu, Z.J. A review on fundamentals for designing oxygen evolution electrocatalysts. *Chem. Soc. Rev.* **2020**, *49*, 2196–2214. [CrossRef] [PubMed]
2. Zhu, B.J.; Xia, D.G.; Zou, R.Q. Metal-organic frameworks and their derivatives as bifunctional electrocatalysts. *Coord. Chem. Rev.* **2018**, *376*, 430–448. [CrossRef]
3. Zou, X.X.; Zhang, Y. Noble metal-free hydrogen evolution catalysts for water splitting. *Chem. Soc. Rev.* **2015**, *44*, 5148–5180. [CrossRef]
4. Zhao, J.; Zhang, J.J.; Li, Z.Y.; Bu, X.H. Recent Progress on NiFe-Based Electrocatalysts for the Oxygen Evolution Reaction. *Small* **2020**, *16*, 2003916. [CrossRef] [PubMed]
5. Antolini, E. Iridium as catalyst and cocatalyst for oxygen evolution/reduction in acidic polymer electrolyte membrane electrolyzers and fuel cells. *ACS Catal.* **2014**, *4*, 1426–1440. [CrossRef]
6. Pi, Y.; Zhang, N.; Guo, S.; Guo, J.; Huang, X. Ultrathin laminar Ir superstructure as highly efficient oxygen evolution electrocatalyst in broad pH range. *Nano Lett.* **2016**, *16*, 4424–4430. [CrossRef]
7. Raman Abhinav, S.; Patel, R.; Vojvodic, A. Surface stability of perovskite oxides under OER operating conditions: A first principles approach. *Faraday Discuss.* **2021**, *229*, 75–88. [CrossRef] [PubMed]
8. Hu, C.; Hu, Y.; Fan, C.; Yang, L.; Zhang, Y.; Li, H.; Xie, W. Surface-Enhanced Raman Spectroscopic Evidence of Key Intermediate Species and Role of NiFe Dual-Catalytic Center in Water Oxidation. *Angew. Chem. Int. Ed.* **2021**, *133*, 19774–19778. [CrossRef]
9. Lee, Y.; Suntivich, J.; May, K.J.; Perry, E.E.; Shao-Horn, Y. Synthesis and activities of rutile IrO_2 and RuO_2 nanoparticles for oxygen evolution in acid and alkaline solutions. *Phys. Chem. Lett.* **2012**, *3*, 399–404. [CrossRef]
10. Gao, M.; Sheng, W.; Zhuang, Z.; Fang, Q.; Gu, S.; Jiang, J.; Yan, Y. Efficient water oxidation using nanostructured α-nickel-hydroxide as an electrocatalyst. *Am. Chem. Soc.* **2014**, *136*, 7077–7084. [CrossRef]
11. Huang, G.; Zhang, C.; Liu, Z.; Yuan, S.; Yang, G.; Li, N. Ultra-small NiFe-layered double hydroxide nanoparticles confined in ordered mesoporous carbon as efficient electrocatalyst for oxygen evolution reaction. *Appl. Surf. Sci.* **2021**, *565*, 150533. [CrossRef]
12. Yu, Z.-Y.; Duan, Y.; Liu, J.-D.; Chen, Y.; Liu, X.-K.; Liu, W.; Ma, T.; Li, Y.; Zheng, X.-S.; Yao, T.; et al. Unconventional CN vacancies suppress iron-leaching in Prussian blue analogue pre-catalyst for boosted oxygen evolution catalysis. *Nat. Commun.* **2019**, *10*, 358–368. [CrossRef]
13. Feng, X.; Jiao, Q.; Cui, H.; Yin, M.; Li, Q.; Zhao, Y.; Li, H.; Zhou, W.; Feng, C. One-Pot synthesis of $NiCo_2S_4$ hollow spheres via sequential ion-exchange as an enhanced oxygen bifunctional electrocatalyst in alkaline solution. *ACS Appl. Mater. Inter.* **2018**, *10*, 29521–29531. [CrossRef]
14. Deng, J.; Ren, P.; Deng, D.; Yu, L.; Yang, F.; Bao, X. Highly active and durable non-precious-metal catalysts encapsulated in carbon nanotubes for hydrogen evolution reaction. *Energy Environ. Sci.* **2014**, *7*, 1919–1923. [CrossRef]
15. Hu, K.; Ohto, T.; Chen, L.; Han, J.; Wakisaka, M.; Nagata, Y.; Fujita, J.-i.; Ito, Y. Graphene Layer Encapsulation of NonNoble Metal Nanoparticles as Acid-Stable Hydrogen Evolution Catalysts. *ACS Energy Lett.* **2018**, *3*, 1539–1544. [CrossRef]
16. Mahmood, J.; Anjum, M.A.R.; Shin, S.; Ahmad, I.; Noh, H.; Kim, S.; Jeong, H.Y.; Lee, J.S.; Baek, J. Baek, Encapsulating Iridium Nanoparticles Inside a 3D Cage-Like Organic Network as an Efficient and Durable Catalyst for the Hydrogen Evolution Reaction. *Adv. Mater.* **2018**, *30*, 1805606. [CrossRef]
17. Chen, Z.; Wu, R.; Liu, Y.; Ha, Y.; Guo, Y.; Sun, D.; Liu, M.; Fang, F. Ultrafine Co Nanoparticles Encapsulated in Carbon-Nanotubes-Grafted Graphene Sheets as Advanced Electrocatalysts for the Hydrogen Evolution Reaction. *Adv. Mater.* **2018**, *30*, e1802011. [CrossRef]
18. Gao, X.; Zhang, H.; Li, Q.; Yu, X.; Hong, Z.; Zhang, X.; Liang, C.; Lin, Z. Hierarchical $NiCo_2O_4$ Hollow microcuboids as bifunctional eectrocatalysts for overall water-splitting. *Angew. Chem. Int. Ed.* **2016**, *128*, 6290–6294. [CrossRef]

19. Cui, X.; Ren, P.; Deng, D.; Deng, J.; Bao, X. Single layer graphene encapsulating non-precious metals as high-performance electrocatalysts for water oxidation. *Energy Environ. Sci.* **2016**, *9*, 123–129. [CrossRef]
20. Zhou, Y.; Chen, W.; Cui, P.; Zeng, J.; Lin, Z.; Kaxiras, E.; Zhang, Z. Enhancing the Hydrogen Activation Reactivity of Nonprecious Metal Substrates via Confined Catalysis Underneath Graphene. *Nano Lett.* **2016**, *16*, 6058–6063. [CrossRef] [PubMed]
21. Liu, Z.; Tan, H.; Liu, D.; Liu, X.; Xin, J.; Xie, J.; Zhao, M.; Song, L.; Dai, L.; Liu, H. Promotion of overall water splitting activity over a wide pH range by interfacial electrical effects of metallic NiCo-nitrides nanoparticle/$NiCo_2O_4$ nanoflake/graphite fibers. *Adv. Sci.* **2019**, *6*, 1801829. [CrossRef]
22. Tong, Y.; Chen, P.; Zhou, T.; Xu, K.; Chu, W.; Wu, C.; Xie, Y. A bifunctional hybrid electrocatalyst for oxygen reduction and evolution: Cobalt oxide nanoparticles strongly coupled to B, N-decorated graphene. *Angew. Chem. Int. Ed.* **2017**, *129*, 7227–7231. [CrossRef]
23. Wang, C.; Yang, H.; Zhang, Y.; Wang, Q. NiFe alloy nanoparticles with hcp crystal structure stimulate superior oxygen evolution reaction electrocatalytic activity. *Angew. Chem. Int. Ed.* **2019**, *131*, 6099–6103. [CrossRef]
24. Hu, L.; Zhang, R.; Wei, L.; Zhang, F.; Chen, Q. Synthesis of FeCo nanocrystals encapsulated in nitrogen-doped graphene layers for use as highly efficient catalysts for reduction reactions. *Nanoscale* **2015**, *7*, 450–454. [CrossRef]
25. Song, Q.; Li, J.; Wang, S.; Liu, J.; Liu, X.; Pang, L.; Li, H.; Liu, H. Enhanced Electrocatalytic Performance through Body Enrichment of Co-Based Bimetallic Nanoparticles In Situ Embedded Porous N-Doped Carbon Spheres. *Small* **2019**, *15*, 1903395. [CrossRef]
26. Sun, H.; Min, Y.; Yang, W.; Lian, Y.; Lin, L.; Feng, K.; Deng, Z.; Chen, M.; Zhong, J.; Xu, L.; et al. Morphological and Electronic Tuning of Ni_2P through Iron Doping toward Highly Efficient Water Splitting. *ACS Catal.* **2019**, *9*, 8882–8892. [CrossRef]
27. Tian, X.; Zhao, X.; Su, Y.-Q.; Wang, L.; Wang, H.; Dang, D.; Chi, B.; Liu, H.; Hensen, E.J.; Lou, X.W.; et al. Engineering bunched Pt-Ni alloy nanocages for efficient oxygen reduction in practical fuel cells. *Science* **2019**, *366*, 850–856. [CrossRef]
28. Kitchin, J.R.; Nørskov, J.K.; Barteau, M.A.; Chen, J.G. Role of strain and ligand effects in the modification of the electronic and chemical Properties of bimetallic surfaces. *Phys. Rev. Lett.* **2004**, *93*, 4–7. [CrossRef]
29. Yang, Y.; Lun, Z.; Xia, G.; Zheng, F.; He, M.; Chen, Q. Non-precious alloy encapsulated in nitrogen-doped graphene layers derived from MOFs as an active and durable hydrogen evolution reaction catalyst. *Energy Environ. Sci.* **2015**, *8*, 3563–3571. [CrossRef]
30. Deng, J.; Deng, D.; Bao, X. Robust catalysis on 2D materials encapsulating metals: Concept, application, and perspective. *Adv. Mater.* **2017**, *29*, 1606967. [CrossRef]